Application of Direct Fluid Flow Oscillations to Improve Mixing in Microbioreactors

X. Li, G. van der Steen, G. W. K. van Dedem, L. A. M. van der Wielen, M. van Leeuwen, W. M. van Gulik, J. J. Heijnen, and M. Ottens
Dept. of Biotechnology, Delft University of Technology, Delft, The Netherlands

E. E. Krommenhoek, J. G. E. Gardeniers, and A. van den Berg
MESA+ Research Institute, University of Twente, Enschede, The Netherlands

DOI 10.1002/aic.11880
Published online July 22, 2009 in Wiley InterScience (www.interscience.wiley.com).

This article describes an active mixing method for a microbioreactor that was designed, simulated, tested, and successfully implemented. By applying a varying pressure to a microchannel looping tangentially into a cylindrical microreactor an oscillating fluid flow was shown to occur. Such an oscillating fluid flow improved mixing, both by diffusion and convection. The oscillating fluid flow has a large impact on the ratio between the diffusion domain and the convection domain. A good match was obtained between experimental mixing results, computational fluid dynamics simulation results and the results of a simplified mixing model thus demonstrating the potential of simulation on improving the design of microreactors. © 2009 American Institute of Chemical Engineers *AIChE J*, 55: 2725–2736, 2009

Keywords: microbioreactor, micromixing, oscillations, computational fluid dynamics (CFD), microfluidics

Introduction

In recent years, there has been a growing interest in developing minute ''laboratories on a chip'' and in microchemical reactors able to perform chemical and biological experiments and analysis. Many industrial companies and research institutes are involved in research into developing microreaction technology. All the parties involved are convinced of the unique possibilities of microreaction technology comprising relatively fast mixing, sufficient heat transfer, sensitive and efficient reaction control, and simple scaling up in principle allowing for environmentally friendly production methods.[1]Some of these microdevices have been produced on commercial production scales, and many more possible designs have been tested on a laboratory scale. For instance, Kostov et al.[2] described a 24-well plate with unit working volume 2 ml micobioreactor, which can be used to study cultivate *Escherichia coli*. Zanzotto et al.[3] developed a batch microbioreactor with volume 5 and 50 μl also for *Escherichia coli* fermentation. Zhang et al.[4,5] utilized an array of four 80 μl fed-batch and continuous microbioreactor for *E. coli* growth. Balagadde et al.[6] demonstrated a 16 nl microchemostat on a chip to monitor a long-term bacteria growth. Doig et al.[7] used three different microplates (24-, 96-, and 384-wells) with working volume 65 and 1182 μl to grow *Bacillus subtilis*. To have those reactors work properly different mixing methods were applied.

Normally achieving a well-mixed situation in a microsystem consumes less energy than in a macro system, and theoretically due to the smaller working volume, it is believed to be easier to control the mixing behavior in a microsystem. However, due to the low Reynolds numbers achievable (<100) on a microscale, mixing in a microfluidic system is typically dominated by diffusion rather than turbulence. Furthermore, mixing by diffusion only may be time-consuming and inefficient.

Improved mixing thus relies on two principles: first the need to create a more chaotic flow on a small scale; second the need to increase the interfacial area between the liquids to achieve fast mixing via diffusion. Most of the research has focused on the second principle, because an

Correspondence concerning this article should be addressed to M. Ottens at m.ottens@tudelft.nl

increase in the diffusion area can easily be achieved by simply changing the mixer geometry while chaotic flow would require the liquids to travel at high velocities and hence energy to be introduced into the flow from an external source.

Microfluidic systems can also be broadly categorized into continuous-flow systems and batch systems. Continuous-flow systems may have either a plug flow reactor (PFR) or a continuous stirrer tank reactor (CSTR) configuration, and have a continuous input liquid flow and an equal output flow. Batch systems utilize isolated volumes of liquid. Within each system mixing can be carried out passively or actively. Passive mixing requires no energy input other than used to drive fluid flow at a constant rate. Active mixing, on the other hand, requires an external actuator, which inputs extra energy to induce chaotic mixing.

Most recent research focuses on continuous operations. With the passive continuous mixer, the basic design is a T-shaped or Y-shaped mixer.[8] Based on this principle, people have developed other types of micromixers that only require structured microchannels. Examples are utilizing surface tension effects to create a time-dependent flow pattern inside a multisample liquid plug as this plug moves through a chamber[9]; repeated dividing and merging of fluids[10,11]; and varying the 3D structure to enhance the convection around bends.[1,12–16] For active mixing, several actuators have been implemented, including, ultrasonic wave induction,[9,17] order-changing microfluidic devices,[18] crosschannel micromixer with oscillatory flow,[19] magnetic stirring[4,5] and piezoelectric lead-zirconate-titanate actuators (PZT),[17] and recently recycle flow mixing.[20]

The most commonly used energy source to drive fluid flow through static mixers is pressure difference, which is very easy to implement and which can be very accurately controlled within a relatively large range. However, the complex structure of the static mixers limits the potential application. For active mixers, the commonly used energy sources are ultrasonic wave, magnetic energy and PZT. All these energies can be created by using small size devices, which is a big advantage for microscale applications. However, reducing the size of those devices to a smaller scale will certainly limit the energy that each individual device can produce. Therefore, most of those active mixers operate at a high frequency. Furthermore, because of the physical limitation of actuators, present active mixing methods can only be scaled down for microreactors, whose working volume are around 100 μl or larger. By combining the advantages of both passive and active mixing strategies, that is a powerful driving force, for example, induced by pressure and a high-frequency operating mode, we expect that an effective new mixing strategy, which is suitable for varies scales can be developed.

In this article, we will demonstrate, both on the basis of computational fluid dynamics (CFD) simulations and their experimental validation, the possibility of applying a pump-based oscillating mixing in a microreactor, which is developed as a fed-batch microbioreactor for microscale fermentations.[21] In what follows, we first briefly describe the model used in the simulation before presenting the simulation results. Subsequently, we describe the experimental system, the experimental results, and the comparison between experiments and simulations. Furthermore, it is validated that this novel mixing method is applicable in yeast cell fermentation, and it has no negative impact on cell viability, contrary to other traditional mixing methods, that is magnetic stirrer mixing.

Materials and Methods

μ-Bioreactor/mixer design and simulation

To optimally design the mixing performance of the microbioreactor, its mixing performance was simulated using the commercially available CFD software package FEMLAB 3.1 (COMSOL, Sweden). A choice needs to be made between active and passive mixing. We chose a passive mixing, as it does not require the installation of moving parts (which is difficult to realize at such small scales). Passive mixing strategies have the advantage of higher reliability because there are no moving parts that would require additional power and control. Nevertheless, to achieve good mixing, most passive mixers have complex structures to increase the diffusion area or enhance convective radial diffusion (Taylor dispersion) in a microchannel. Such unique passive structures may limit the use of the mixer, especially in a multiphase system. Therefore, to avoid such a complex structure, a simple cylindrical microreactor was used, as shown in Figure 1. A pressure difference is induced in the microchannel, which is connected to the bottom port of the reactor (Boundary 5, Figure 2). A square wave pressure oscillation with a certain frequency and amplitude is imposed on the inlet (Figure 3a). Under different pressures, a solution, which resides in the microchannel and the reactor, is pushed out of the microreactor into the channel or vice versa. The movement of the solution follows the square wave in phase with the pressure

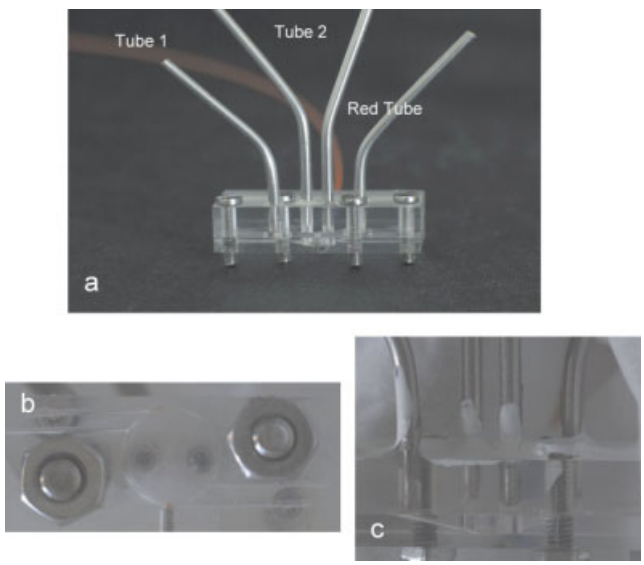

Figure 1. Microreactor (a) overall picture of the microreactor, (b) bottom view of the microreactor, and (c) side view of the microreactor.

[Color figure can be viewed in the online issue, which is available at www.interscience.wiley.com.]

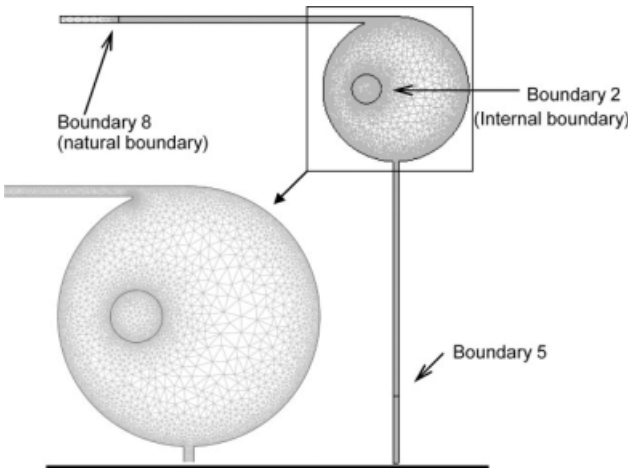

Figure 2. Simulation grids and 2D simulation geometry.

variation. This alternating fluid motion induces convection in the reactor, thus improving the mixing in the reactor. To investigate the mixing performance of the proposed mixing mode, FEMLAB 3.1 was used for a CFD analysis. The physical properties of water were applied in the simulation. The diffusion coefficient of the dye in an aqueous solution was set to 3.5×10^{-10} m^2 s^{-1}.[22] To simplify the simulation, initially a 2D simulation was selected instead of a full 3D simulation. Because of the limited height of the reactor of only 1/3 to 1/4 of the reactor diameter, a bottom view (Figure 1b) shows the extent of mixing more clearly than the side view (Figure 1c). Therefore, the bottom view geometry of the reactor was used in the simulation as shown in Figure 2.

Only tube 1 was open during the experiments, all the other three tubes were sealed, therefore, in the simulation, tube 1 was the only tube included.

The model uses the *Incompressible Navier–Stokes* equations and the *Convection and Diffusion* equation. The model equations are formulated as following.[23]

$$\rho\frac{\partial U}{\partial t} - \nabla \cdot \left[\eta \cdot \left(\nabla U + (\nabla U)^T\right)\right] + \rho U \cdot \nabla U + \nabla P = F$$
$$\nabla \cdot U = 0 \quad (1)$$

$$\frac{\partial c_i}{\partial t} + \nabla \cdot (-D_i \nabla c_i + c_i U) = R_i \quad (2)$$

In the aforementioned equations, η denotes the dynamic viscosity of the solution (kg m^{-1} s^{-1}), U denotes the velocity vector (m s^{-1}), ρ denotes the density (kg m^{-3}), P is the pressure (Pa), c_i denotes the concentration of chemical i in solution (kg m^{-3}), D_i denotes its diffusion coefficient, and R_i denotes the reaction term (kg s^{-1} m^{-3}). F denotes the selected volume force field (i.e. gravity), which influences the velocity field (N m^{-3}). The expression within brackets in Eq. 2 represents the flux vector, where the first term describes the transport by diffusion and the second represents the convective flux.

The oscillation term in the simulation was set on Boundary 5 (Figure 2), by using the following formula:

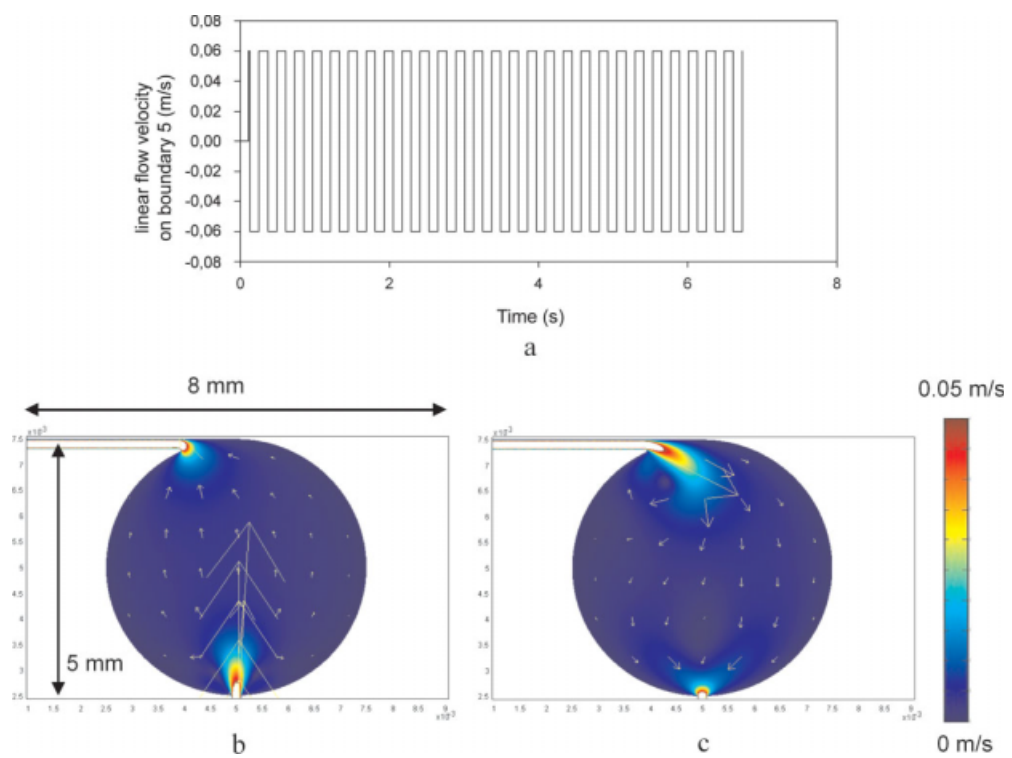

Figure 3. (a) Linear flow rate on Boundary 5 during the simulation, (b) velocity field in the reactor when Boundary 5 has a positive value, and (c) velocity field in the reactor when Boundary 5 has a negative value.

[Color figure can be viewed in the online issue, which is available at www.interscience.wiley.com.]

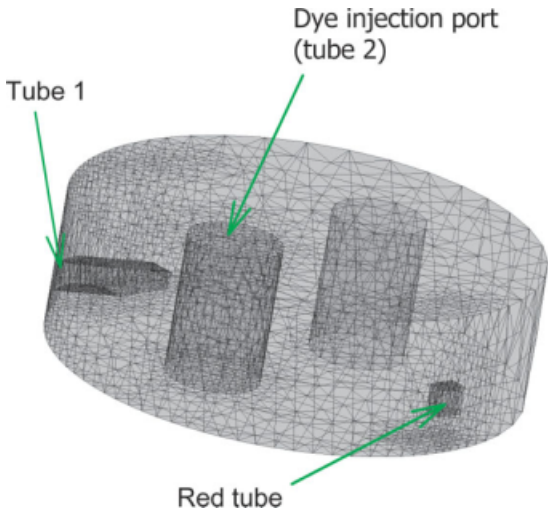

Figure 4. Simulation grids and 3D simulation geometry.

[Color figure can be viewed in the online issue, which is available at www.interscience.wiley.com.]

$$U = v_1 - 2 \cdot v_1 \cdot f_{\mathrm{HS},c_1}(x, x_{\max}) \tag{3}$$

$$x = \sin\left(\frac{a \cdot t}{\pi}\right) \tag{4}$$

In the aforementioned equations, U denotes the linear flow rate on the set boundary in m s^{-1}. v_1 denotes the maximum linear flow rate of the pushing flow in m s^{-1}. t denotes the time in seconds. a is a constant, which helps to convert time t into the frequency function to the certain time interval. The function $f(x) = f_{\mathrm{HS},c_1}(x, x_{\max})$ is used to calculate the value of the smooth version of the Heaviside function (e.g., Ref. 24). The function is 0 at $x < -x_{\max}$ and 1 at $x > x_{\max}$. In the interval of $-x_{\max} < x < x_{\max}$, $f_{\mathrm{HS},c_1}(x, x_{\max})$ is a smooth Heaviside function with a continuous first derivative without overshoot, defined by a fifth-order polynomial. Boundary 2 was set as the internal boundary, which had no influence on the main part of the simulation, but only helped the dye injection simulation. Boundary 8 was set as natural boundary, which is used to balance the velocities of the overall system.

Two different parameters were discussed in the simulation, as mentioned previously, one was the set velocity in m s^{-1}, and the other was the oscillation period in seconds.

As shown in Figure 2, for the designed geometry 14,471 nodes were used in the simulation. The degree of freedom is 98,976. For a simulated operating time of 10 s, it took around 20,000 s CPU time in a 3 GHz microprocessor.

Figure 4 shows the geometry of the full 3D simulation. To reduce the simulation complexity, only the reactor part was included in the simulation. The model also uses the *Incompressible Navier–Stokes* equations and the *Convection and Diffusion* equation. The oscillation term was set as same as the 2D model. Finer meshes (triangle) were set around two oscillation ports and dye injection spot. Coarser meshes were used for the major part of the reactor to reduce the amount of the nodes. In total, 23,662 nodes were used in the simulation. The degree of freedom is 148,547. For a simulated operating time of 1 s, it took more than 12,000 s CPU time in a 3 GHz microprocessor.

Chemicals

All reagents were analytical grade. Rhodamine B powder was supplied by SIGMA company (Steinheim, Germany). $(NH_4)_2SO_4$, KH_2PO_4 and $MgSO_4$-$7H_2O$ were purchased from Baker Analyzed reagent (Deventer, The Netherlands). All solutions were prepared with doubly distilled water and passed through a 0.22 μm cellulose acetate filter (Molshelm, France). To prepare the pH 4 buffer solution, 2.5 g $(NH_4)_2SO_4$, 1.5 g KH_2PO_4, and 0.51 g $MgSO_4$-$7H_2O$ were dissolved into 50 ml deionized water. One millimolar Rhodamine B solution was prepared by dissolving 1.2 g Rhodamine B power into 30 ml buffer solution. Two milliliters of fermentation broth was taken from a 4 l batch fermentation culture, which was started from overnight grown of a preculture (0.5 l) of *Saccharomyces cerevisae* in a shake flask at 30°C on pH 4 buffer and sufficient glucose feeding.[25] Dry weight of cell culture was around 15 g l^{-1}.

Microbioreactor

Photographs of the microreactor are shown in Figure 1. The reactor consisted of two parts: the lid layer and the reactor layer. Both layers were made of poly(dimethylsiloxane) PDMS. For the reactor layer, the main reactor volume was drilled out by using a 5 mm diameter flat surface drilled on a PDMS plate. Using a 0.1 mm driller, several side channels with a diameter of 100–120 μm were drilled in the reactor plate. A red polyetheretherketone (PEEK) polymer tubing was connected to the bottom port of the reactor. Four metal tubes were fixed to the lid layer. Tubes 1 and 4 were connected to the side channels of the reactor. Tubes 2 and 3 were placed above the central reactor axis. The microreactor had a diameter of 5 mm, a height of 1.5 mm and a volume of 27 μl. The side channels had a diameter of ~300–500 μm. The backside port diameter was 800–1200 μm. The two layers were placed on top of each other and secured with four screws.

Additional equipment

A Leica DFC 280 digital camera (Heerbrugg, Germany), a KD-scientific S-101 syringe pump (USA), a Single stirrer motor (RET B, IKA Werke, Germany) and a Leica Qwin image control and analysis program were used in this work.

Experimental procedure

Microbioreactor Mixing Experiment. To characterize the actual mixing in the microreactor, 1.5 μl of a solution of Rhodamine red B dye in demineralized water was injected into the reactor via tube 2. Subsequently, by continuously running the oscillating syringe pump, which was connected to the red PEEK tube, the dye was dispersed. The syringe pump displaced a fixed volume (2 μl) at a fixed pumping rate. The digital camera was used to record on video the mixing performance by measuring the change in color distribution in the reactor. Thus, at the beginning of the experiment only the injected dye spot showed up as a red spot.

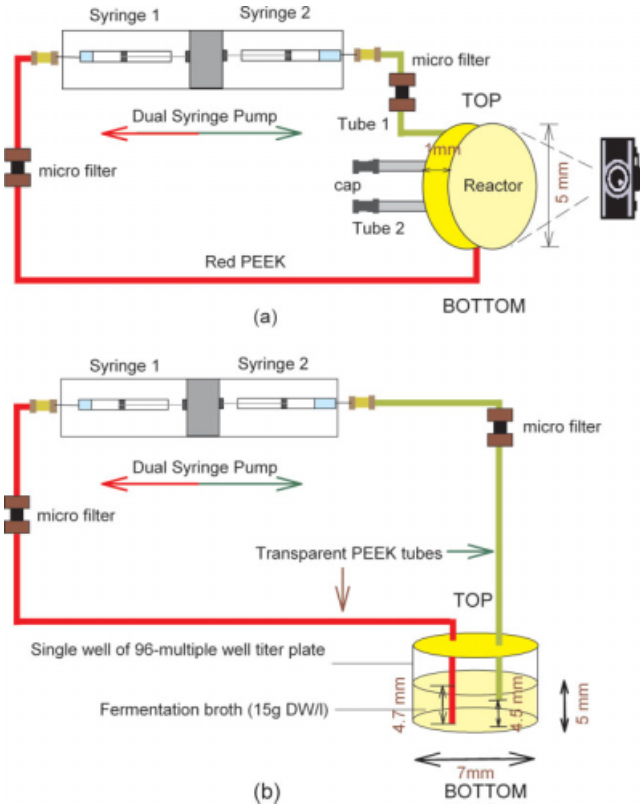

Figure 5. Schematic representation of experimental setup: (a) cell settling experiment with 27 μl microbioreactor and (b) cell settling experiments with single well from 96 multiple well titer plate.

[Color figure can be viewed in the online issue, which is available at www.interscience.wiley.com.]

During the oscillation, the dye was dispersed to the other parts of the reactor. One of the driving forces for dye dispersion is the dye concentration gradient (diffusion), but more importantly, the dye's dispersion was caused by the oscillation-induced convection flow. At the end of the experiment, the color in the reactor was the same everywhere, indicating that the dye was homogeneously distributed in the reactor. The color density of the images was measured and it showed that mixing was achieved after a certain time.

Cell Settling Experiment. Fermentation broth was filled into microreactor, a microfilter was placed between the PEEK tube and the syringe pump to keep the cells inside the reactor and PEEK tubes. The reactor was placed vertically as illustrated in Figure 5a. The oscillation syringe pump displaced a fixed volume (2 μl) at a fixed pumping rate (1000 μl min^{-1}). The oscillation mixing was started and kept overnight.

The cell settling issue was additionally tested in a single well of a 96 multiple well titer plate as shown in Figure 5b. First, two transparent PEEK tubes were placed in the well and connected to two syringes, fixed on opposite sides of an oscillation pump. Second, the well was filled with 200 μl fermentation broth, and the oscillation pump was set to a fixed displacement volume (10 μl) at a fixed pumping rate (1000 μl min^{-1}). The oscillation mixing was started and kept overnight. At the end of the experiment, 2 μl fermentation broth was taken from the well and was placed under a microscope equipped with the aforementioned CCD camera to take pictures of *S. cerevisae*.

For comparison, a micromagnetic stirrer bar experiment was performed. 200 μl fermentation broth was filled into a single well of a 96 multiple well titer plate. The well was closed using a rubber cap. A hole was drilled in the magnetic stainless steel stirrer bar of 1.67 mm × 2.01 mm × 4.80 mm dimensions (VP 711-1, V&P Scientific, Netherlands). A needle was pinched through the center point of the rubber cap. The tip of the needle was bent as to fixate the stirrer bar at elevated height. The mixing started with a fixed speed 600 rpm. After 4 h mixing, 2 μl fermentation broth was taken from the well and was placed under a microscope equipped with the aforementioned CCD camera to take pictures of *S. cerevisae*.

Data processing

The mixing performance of the oscillating flow in the reactor can be quantitatively analyzed from the recorded pictures. However, unlike in the static mixer, which uses outlet concentration against inlet concentration to indicate the mixing performance, the quantitative analysis in this case uses a factor called *colored area ratio*. This *colored area ratio* is defined as A_t/A_f. A is the colored area size in square meter, subscript "t" is the time in s, and subscript "f" is indicates the equilibrium condition at the final state. The colored area is defined as the area where the dye has a more intense color than the final state color. Because the color intensity is directly related to the *Rhodamin B* concentration, the colored area is actually the area where the dye solution has a higher concentration than in the final state. One thing that needs to be noted is that for every single picture, the color intensity is influenced by the noise from the surrounding, which is mainly the slight change in light during the experiment. To eliminate the influence of that background, light change is monitored and it is excluded from the measured color intensity.

Results

Simulation results

As mentioned in the simulation procedure, two parameters were set in the simulations, that is, the maximum linear flow velocity on Boundary 5 and the switching time. In Figure 6, the results are shown for a linear flow velocity of 0.06 m s^{-1} ($v_1 = 0.06$), and a switching time of 0.12 s ($a = 83$). The reactor very easily achieved complete mixing within 4 s. The mixing in the overall reactor system can be divided into two parts. The first part is the mixing inside the reactor unit where, due to the unevenly distributed flow velocity field, as shown in Figures 3b, c, a larger dye-influenced area was obtained (Figure 6). The main mixing mechanism in this part of the system is convection based dispersion. The second part is the mixing in the microchannel, which follows a two-directional Taylor dispersion. Taylor dispersion arises from the velocity profile near the channel walls due to the no-slip flow condition at the

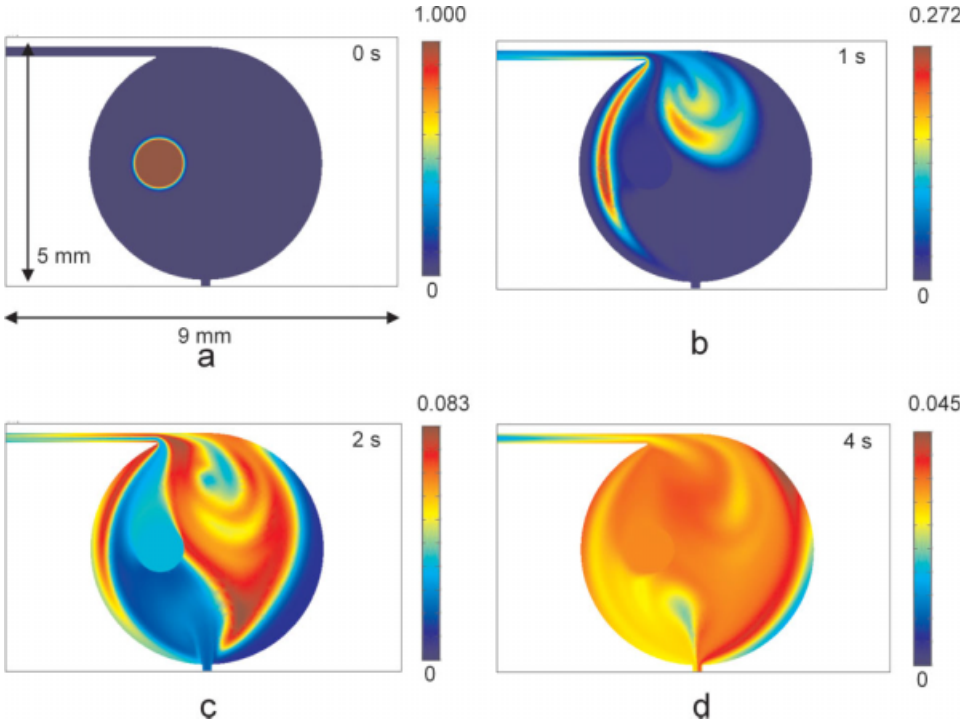

Figure 6. Simulation result of the concentration profile of oscillation mixing in the reactor at different times with the flow velocity set at 0.06 m s^{-1} and the oscillation frequency 8.33 Hz; (a) t = 0 s, (b) t = 1 s, (c) t = 2 s, and (d) t = 4 s.

[Color figure can be viewed in the online issue, which is available at www.interscience.wiley.com.]

solid-fluid interface.[26,27] Obviously, the velocity profile will significantly contribute to the mixing behavior.[12,28]

The Taylor–Aris dispersivity (K) is used to describe the impact of the Taylor dispersion compared with the molecular diffusion. The Taylor–Aris dispersivity (K) for pressure-driven flow between two parallel plates is given as[29]:

$$\frac{K}{D} = 1 + \frac{1}{210}\left(\frac{Ud}{D}\right)^2 \tag{5}$$

where D is the molecular diffusion coefficient of the species (m^2 s^{-1}), U is the average fluid velocity (m s^{-1}), and d is the separation distance between the parallel plates (m). The aforementioned expression indicates that the overall mass transfer in the pressure-driven system arises from two additive contributions, diffusion transport in the flow direction (the first term of the equation) and the effective dispersivity due to the fluid shear (the second term of the equation). The latter term of the equation scales with the square of the Peclet number Ud/D, which estimates the relative magnitude of convection to diffusive transport rates in the system. The coefficient multiplying this dimensionless group in the aforementioned equation is a function of the channel cross-section and has a value of 1/210 for two parallel plates. For a closed microchannel, it is important to note that the exact cross-section of the channel can significantly affect the actual dispersion. Mathematically, that effect can be evaluated by introducing a function f in Eq. 5 as[26]:

$$\frac{K}{D} = 1 + f\left(\frac{Ud}{D}\right)^2 \tag{6}$$

The factor f relates to the shape of the channel cross-section. The effect of the typical microchannel cross-sections geometry on the hydrodynamic dispersion of the solution slugs has been well investigated in the past.[26,30,31] These studies have shown that the function f for this profile increases monotonically with an increase in the aspect ratio of the conduit. For a square cross-section, which is close to our geometry, $f \approx 1.76$.[26] On our microfluidic devices, because the diffusion coefficients for most analytes have values smaller than 10^{-5} cm^2 s^{-1}, with channels having a diameter around 100 μm, linear flow rates larger than 1 cm s^{-1}, K/D ratio has a value larger than 10^4, which indicates the dispersivity of the chemical significantly exceeds its diffusional limit ($K/D = 1$).

Two-directional Taylor dispersion gives very good mixing as shown in Figure 7a, which means that within one oscillating cycle, the dye concentration was already more homogeneously dispersed as shown in Figure 7b. Figure 8 clearly shows that the mixing time in the reactor decreases as the pulling and pushing flow velocity increases due to the impact of the increase in energy input. With a linear flow rate of 0.02 m s^{-1} and an oscillation frequency 8.33 Hz, well mixing can be obtained within 10 s. However, the energy input is not the only factor that has an impact on this mixing method. The positions of the oscillation tubes also

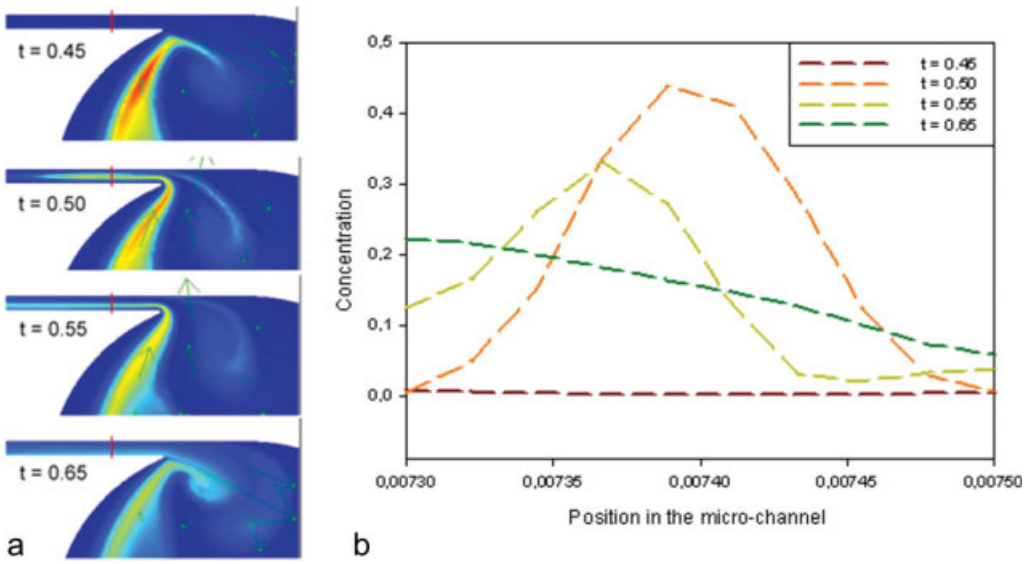

Figure 7. Simulation result of oscillation mixing in the microreactor close to the microchannel inlet part for one pulling and pushing cycle: (a) simulation results displaying the concentration field and (b) time dependant concentration profile along the cross-sectional line in the microreactor.

[Color figure can be viewed in the online issue, which is available at www.interscience.wiley.com.]

play an important role. During reactor design, it is necessary to make sure that the flow field evenly covers most area of the reactor, leaving minimal room for dead zones within the reactor.

The full 3D simulation results are shown in Figure 9, the streamline plots from the top view (Figure 9c) and the side view (Figure 9d) were compared. The parallel streamlines along the *z*-axis shown in Figure 9d indicate that in the most part of the reactor the flow velocity is evenly distributed along the *z*-axis. That is also proved by the flow velocity profile shown in Figure 9b. In the overall reactor only the spaces near the input port and output port are different, and it is caused by the size difference between the reactor and oscillation tube. In other words, the 3D simulation shows the validity of using 2D simulation to simplify this 3D geometry. Of course because of the size difference between the

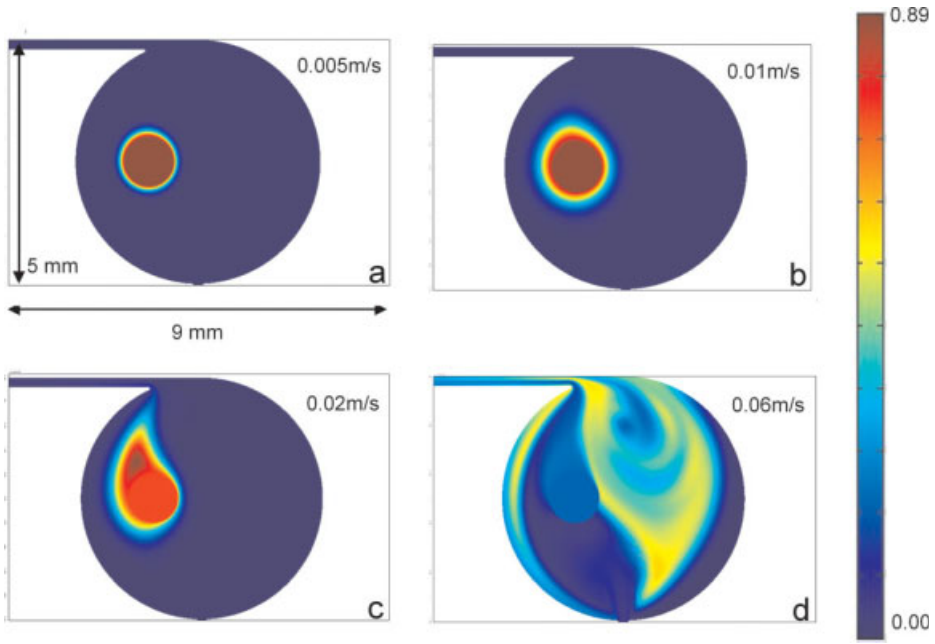

Figure 8. Simulation results of concentration profile of the oscillation mixing with different pulling and pushing linear flow rates; (a) 0.005 m s^{-1}, (b) 0.01 m s^{-1}, (c) 0.02 m s^{-1}, and (d) 0.06 m s^{-1} with same oscillation frequency 8.33 Hz at time 2 s.

[Color figure can be viewed in the online issue, which is available at www.interscience.wiley.com.]

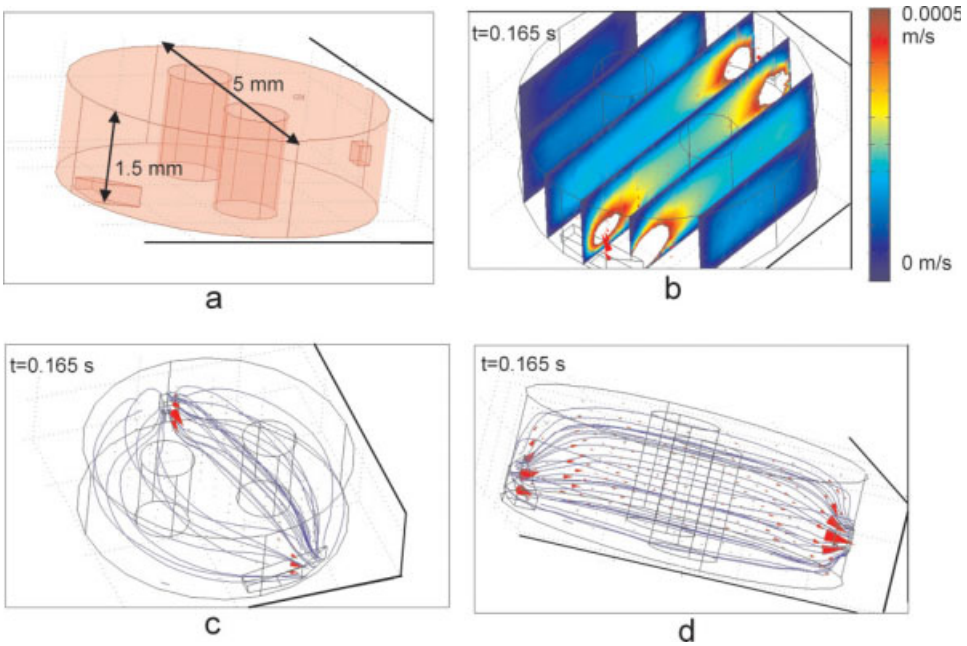

Figure 9. Three-dimensional simulation results for oscillation linear flow rate 0.01 m s^{-1}, frequency 8.33 Hz: (a) simulated geometry, (b) linear flow velocity profile at time 0.165 s, (c) streamline profile on velocity field at time 0.165 s (top view), and (d) streamline profile on velocity field at time 0.165 s.

[Color figure can be viewed in the online issue, which is available at www.interscience.wiley.com.]

reactor and the oscillation tubes, 2D simulation may lose some details, and the simulated result deviates from the experimental one, however, the simulated result still represents sufficient fluid flow information in the reactor and in the oscillation tube.

Experimental results

Figure 10 shows the comparison between the experimental results with an oscillating flow rate of 1000 μl min^{-1} (linear flow rate ~0.015 m s^{-1}) and an oscillation frequency of 8.33 Hz and the simulation results with a fixed maximum linear flow rate of 0.02 m s^{-1} and an oscillation frequency of 8.33 Hz. The correlation between A_t/A_f and time was used to characterize the micromixing. The mixing time was defined as the time to reach an A_t/A_f value of >95%. Figure 11 clearly shows that with a certain oscillation volume, the higher the pumping flow rate, the faster complete mixing will be achieved. The experimental mixing times are shown in Table 1.

It is also possible to use a simplified method to estimate the mixing time in the microreactor by using a micromixing equation[32]:

$$t_{\text{micro}} = 0.1\frac{\lambda_k^2}{D} = 0.1\frac{v^{3/2}}{\varepsilon^{1/2}D} \tag{7}$$

where t_{micro} denotes the mixing time in the microscale system in seconds; λ_K denotes the Kolmogorov length scale in meters; D denotes the diffusivity in the liquid phase in m^2 s^{-1}; v denotes the kinematic viscosity in m^2 s^{-1}; ε denotes the energy dissipation rate in W kg^{-1}.

The kinematic viscosity (v) can be calculated by:

$$v = \frac{\eta}{\rho} \tag{8}$$

where η is the viscosity of the solution in kg m^{-1} s^{-1}; ρ denotes the density of the solution in kg m^{-3}.

The energy dissipation rate (ε) is defined as the energy input per kilogram solution, therefore, it can be estimated from:

$$\varepsilon = \frac{E_{\text{Diss}}}{V_R \cdot \rho} = \frac{E \cdot f}{V_R \cdot \rho} = \frac{\frac{1}{2} \cdot m \cdot v^2 \cdot f}{V_R \cdot \rho} = \frac{\frac{1}{2} \cdot V_{IN} \cdot \rho \cdot v^2 \cdot f}{V_R \cdot \rho} = \frac{V_{IN} \cdot v^2 \cdot f}{2 \cdot V_R} \tag{9}$$

where E_{Diss} denotes the energy dissipation in Watt, E denotes the kinetic energy of the injected fluid in joule, f denotes the frequency in hertz, m denotes the mass of injected liquid in kilograms, V_R is the volume of the reactor in cubic meters, V_{IN} is the injected volume per cycle in cubic meters, and v is the linear flow rate around the port in m s^{-1}. The mixing time can be estimated on the basis of the aforementioned equations. The results are given in Table 1.

Figure 12 compares the results from the 2D CFD simulation, the oscillation mixing experiments and the micromixing model correlation. A good match was obtained, especially within the high energy input range. However, a somewhat larger deviation was observed around the low energy input range. This can be partly explained by the fact that the influence of the dead-zone areas, which was obviously not taken into account in the micromixing correlation, has a larger impact in the low energy input range. Within the dead-zone

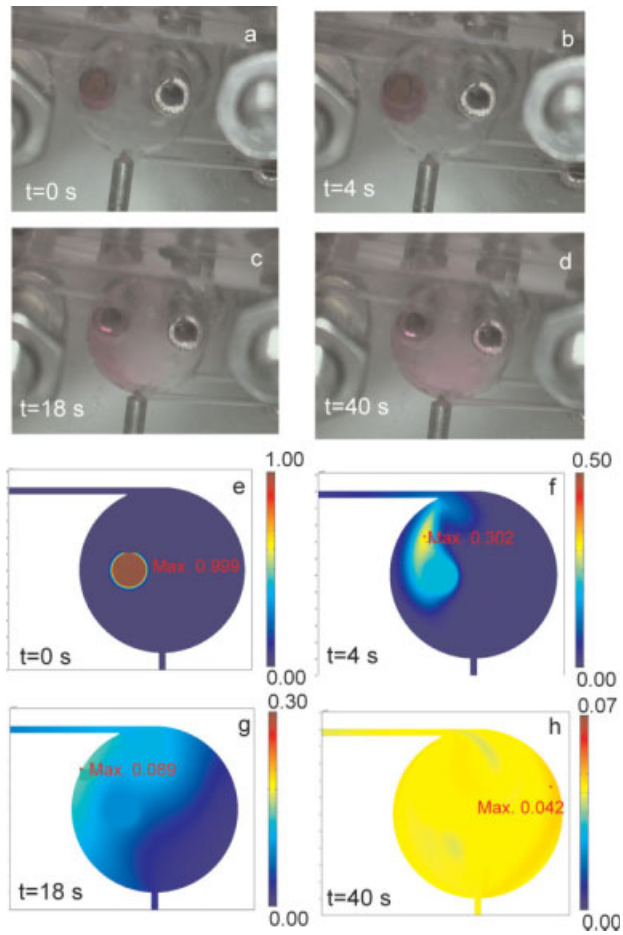

Figure 10. Comparison between the experimental result (f = 8.33 Hz) and simulation result (0.02 m s^{-1}; 0.12 s): (a) t = 0 s, (b) t = 4 s, (c) t = 18 s, (d) t = 40 s, (e) t = 0 s, (f) t = 4 s, (g) t = 18 s, and (h) t = 40 s.

[Color figure can be viewed in the online issue, which is available at www.interscience.wiley.com.]

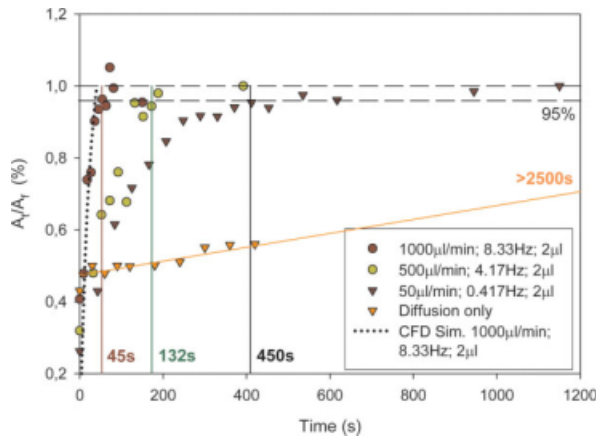

Figure 11. Experimental oscillatory microreactor mixing, different symbols indicate different frequencies and different flow rates.

[Color figure can be viewed in the online issue, which is available at www.interscience.wiley.com.]

Table 1. Comparison of Results of Mixing Times from Oscillation Mixing Measurement, a Simplified Micromixing Correlation and CFD Simulation Results

Mixing Time (s)	Flow Rate (μl min^{-1}) [and Corresponding Oscillation Frequency (Hz)]			
	0* (0)	50 (0.42)	500 (4.17)	1000 (8.33)
Experimental	>2500	412	132	45
Correlation	17,860	698	70	35
FEMLAB simulation (2D)	16,600	–	–	37

*Diffusion only.

areas, diffusion instead of convection takes a dominant role in the mass transfer mechanism.

The experimental curves (50 μl min^{-1}) given in Figure 11 indicate that the oscillation mixing process may have two different periods. In the first period rapid mixing takes place, and the A_t/A_f value ($27\% < A_t/A_f < 90\%$) shows a sharp increase (slope = 2.5×10^{-3} per second). In the second period, the A_t/A_f value still increases ($90\% < A_t/A_f, < 100\%$) but with a smaller slope (9×10^{-5} per second). For the 1000 μl min^{-1} curve, only the rapid increase period was observed. Furthermore, for the 500 μl min^{-1} curve, a much shorter second period ($95\% < A_t/A_f < 100\%$) was observed. From the illustrations earlier, it can be concluded that the fraction of the first period in the total mixing process increased as the oscillating flow rate increased. In other words, the slope of A_t/A_f vs. time curve increased with an increase in the convection flow rate, which proves that during the first period convection is the dominant factor that affects mixing. Furthermore, during the second period diffusion is the dominant factor, because the slope in the second period is close to the slope of the diffusion only curve (2×10^{-4} per second).

For fermentation broths, it is possible to treat yeast cells as very small particles, which means the cells will follow

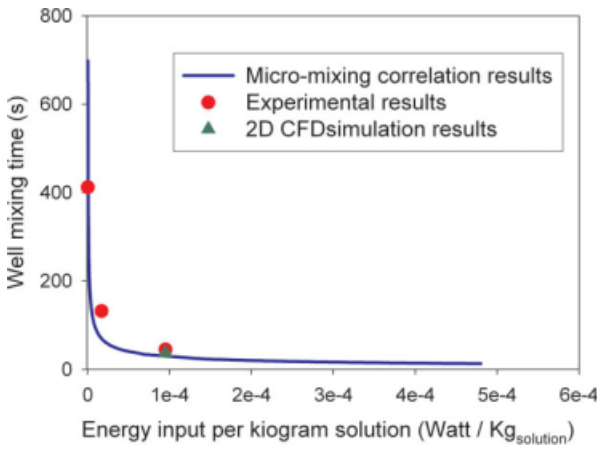

Figure 12. Comparison of results of mixing times from oscillation mixing experiments and a simplified micromixing correlation and 2D CFD simulations.

[Color figure can be viewed in the online issue, which is available at www.interscience.wiley.com.]

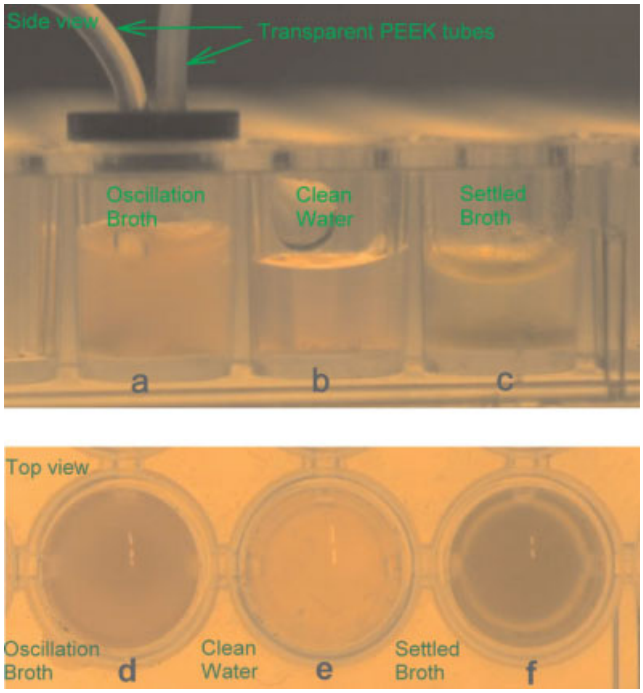

Figure 13. Experimental results of cell settling test for single well: (a) side view of oscillated fermentation broth after overnight mixing with oscillation flow rate 1000 μl min^{-1}, frequency, 1.66 Hz; (b) side view of clean water; (c) side view of settled fermentation broth after overnight stand still; (d) top view of oscillated fermentation broth after overnight mixing with oscillation flow rate 1000 μl min^{-1}, frequency, 1.66 Hz; (e) top view of clean water; and (f) top view of settled fermentation broth after overnight stand still.

[Color figure can be viewed in the online issue, which is available at www.interscience.wiley.com.]

the streamlines in the microbioreactor. The dispersion of the cells within the reactor will mainly be based on convection. Figure 11, clearly indicates that although in the microreactor dye dispersion normally is due to both diffusion and convection, convection takes the dominant place especially under a high-oscillation frequency. Therefore, both dye and the cells will follow the convective patterns (flow field) in the reactor. Thus, good convective dye mixing indicates good yeast cell mixing.

In the microbioreactor, after overnight mixing, many cells kept suspended. This can be explained by the fact that there is <5% density difference between *S. cerevisae* and water. Therefore, with flow oscillation on the bottom of the reactor, which, in this case, is the oscillation around the PEEK port, cells gain sufficient lift to stay suspended. One thing needs to be noted is that because of the large distance between the top of the reactor and bottom of the reactor well (5 mm), and the relatively small oscillation area, the experiment with yeast concentrations of 15 g l^{-1} dry weight showed small areas with slightly higher cell concentrations than the rest of the reactor well. However, by switching the position of the

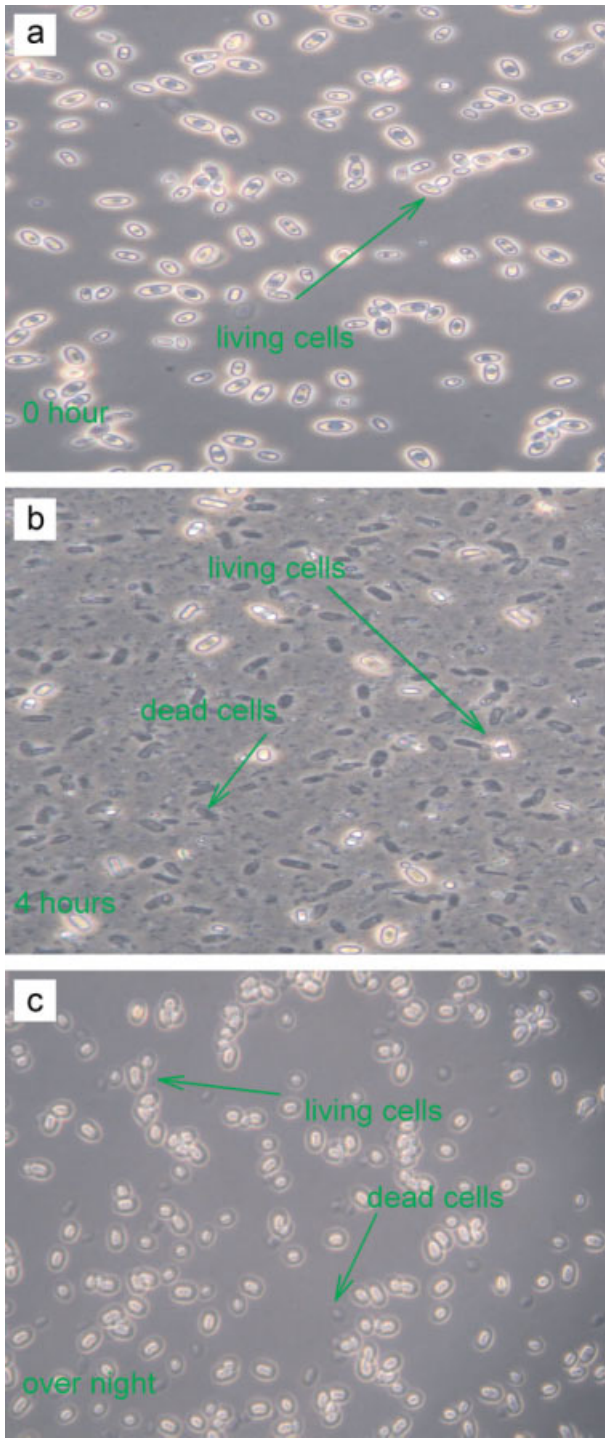

Figure 14. Experimental results of cell viability tests: (a) original fermentation broth, (b) fermentation broth after 4 h vigorous mixing with magnetic stirrer (600 rpm), (c) fermentation broth after overnight oscillation mixing in single well of 96 multiple well titter plate with oscillation flow rate 1000 μl min^{-1}; frequency 1.66 Hz; light cells indicate living cells, dark cells indicate dead cells.

[Color figure can be viewed in the online issue, which is available at www.interscience.wiley.com.]

oscillation tube as illustrated in Figure 5b, during overnight mixing a more or less homogeneous cell suspension was maintained in the microbioreactor as shown in Figure 13.

In Krommenhoek's work,[21] serious cell damage was reported, caused by the vigorous mixing (400–1200 rpm) of a magnetic stirrer in a single well of a 96 multiple well titer plate. Figure 14 shows the comparison of cells condition between the overnight oscillation mixing and 4 h magnetic stirrer mixing (600 rpm). It clearly indicates that more than 80% of the cells were broken after four hours magnetic stirrer mixing. In contrast, barely any cell breakage was observed after overnight mixing with the oscillation mixing method. Furthermore, a relatively long mixing time might not be a problem as long as the mixing prevents cell settling and the transport within the reactor of substrate and oxygen does not become limiting.

Conclusion

In this article, a simple active mixing method for a microbioreactor using a pressure-based oscillating driving force was designed, simulated and tested. Good mixing performance was achieved under high oscillating flow conditions. The experimental results show a reasonably good match with the simulated results and the model-based calculated results. The mixing performance shows that both diffusion and convection contribute to mixing, however, with a large oscillating flow rate the contribution from convection predominates. This method can be easily implemented on most simple microdevices in the volume range several to hundreds microliter, without requiring any complex structures. No extra internal apparatus like stirrer bar or PZT crystal is needed. This method can be easily implemented for multiple parallel reactors, a single central oscillation source is enough to create oscillation flow in different reactors. Furthermore, the position of the oscillation tubes definitely helps to prevent possible cell settling. Compared with the most commonly used microbioreactor mixing method, that is magnetic stirring, the effect of the oscillating flow on cellular viability and behavior is considered to be not a problem, as the oscillation flow induced shear stress is not strong enough to damage the cells.

Acknowledgments

This work is part of the ACTS-IBOS program (IBOS 053.63.009), which is funded by the Dutch Science Foundation (NWO), DSM Anti-Infectives BV, Organon, and Applikon BV.

Notation

a = constant
A = the color area size, m^2
c_i = concentration of chemical i in solution, kg m^{-3}
d = separation distance, m
D_i = diffusion coefficient, m^2 s^{-1}
Diss = dissipation power, W
E = kinetic energy of the injected fluid, J
f = frequency, Hz
F = select volume force field, N
K = Taylor–Aris dispersivity, m^{-3} s^{-1}
m = mass of injected liquid, kg
p = pressure, Pa
R_i = reaction term for species i, kg s^{-1} m^{-3}
t = time, s
t_{micro} = the well mixing time, s
u = velocity, m s^{-1}
U = average fluid velocity in the channel, m s^{-1}
v = linear flow rate around the port, m s^{-1}
v_0 = the linear flow rate on the set boundary, m s^{-1}
v_1 = the maximum linear flow rate of the pushing flow, m s^{-1}
V_{IN} = inject volume per cycle, m^3
V_R = volume of the reactor, m^3

Greek letters

ε = energy dissipation rate, W kg^{-1}
η = dynamic viscosity, kg m^{-1} s^{-1}
λ_K = Kolmogorov length scale, m
ρ = density, kg m^{-3}
ν = kinematic viscosity, m^2 s^{-1}

Literature Cited

1. Ehrfeld W, Golbig K, Hessel V, Lowe H, Richter T. Characterization of mixing in micro mixers by a test reaction: single mixing units and mixer arrays. *Ind Eng Chem Res*. 1999;38:1075–1082.
2. Kostov T, Harms P, Randers-Eichhorn L, Rao G. Low-cost microbioreactor for high-throughput bioprocessing. *Biotechnol Bioeng*. 2001;72:346–352.
3. Zanzotto A, Szita N, Boccazzi P, Lessard P, Sinskey AJ, Jensen KF. Membrane-aerated microbioreactor for high-throughput bioprocessing. *Biotechnol Bioeng*. 2004;87:243–254.
4. Zhang Z, Szita N, Boccazzi P, Sinskey AJ, Jensen KF. Monitoring and control of cell growth in fed-batch micro bio-reactors. *Seventh International Conference on Miniaturized Chemical and Biochemical Analysis Systems*, California, 2003.
5. Zhang Z, Perozziello G, Szita N, Boccazzi P, Sinskey AJ, Geschke O, Jensen KF. *Microbioreactor "Cassette" with integrated fluidic and optical plugs for high-throughput bioprocessing. Proceedings of Micro Total Analysis Systems*, Boston, Massachusetts, 2005.
6. Balagaddé Frederick K, Lingchong Y, Carl L, Arnold HFH, Quake SR. Long-term monitoring of bacteria undergoing programmed population control in a microchemostat. *Science*. 2005;309:137–140.
7. Doig SD, Pickering SCR, Lye GJ, Baganz F. Modelling surface aeration rates in shaken microtitre plates using dimensionless groups. *Chem Eng Sci*. 2005;60:2741–2750.
8. Zhao Y, Chen G, Quan Y. Liquid-liquid two-phase mass transfer in the T-Junction microchannels, *AIChE J*. 2007;53:3042–3053.
9. Monnier H, Willhelm AM, Delmas H. The influence of ultrasound on micromixing in a semi-batch reactor. *Chem Eng Sci*. 1999;54: 2953–2961.
10. Kim DS, Lee SW, Kwon TH, Lee SS. Barrier embedded chaotic micromixer. *IEEE, The Sixteenth Annual International Conference on Micro Electro Mechanical Systems*, Kyoto, Japan, 2003:19–23.
11. Kirner T, Albert J, Gunther M, Mayer G, Reinhackel K, Kohler JM. Static micro mixers for modular chip reactor arrangements in two-step reactions and photochemical activated processes. *Book of Abstracts*. *IMRET 7th International Conference on Microreaction Technology*, Lausanne, Switzerland, 2003:101–105.
12. Hong CC, Choi JW, Ahn CH. A novel in-plane passive microfluidic mixer with modified tesla structures. *Lab Chip*. 2004;4:109–113.
13. Nguyen NT, Wu Z. Micromixers—a review. *J Micromech Microeng*. 2005;15:R1-R16.
14. Kolbl A, Kraut M, Schubert K. The Iodide Iodate method to characterize microstructured mixing devices. *AIChE J*. 2008;54:639–645.
15. Liu R, Stremler HMA, Sharp KV, Olsen MG, Santiago JG, Adrian RJ, Aref H, Beebe DJ. Passive mixing in a three-dimensional serpentine micro-channel. *J Micro Electromech Syst*. 2000;9:190–197.
16. Schwesinger N, Frank T, Wurmus H. A modular microfluid system with an integrated micromixer. *J Micromech Microeng*. 1996;6: 99–102.
17. Zhen Y, Matsumoto S, Goto H, Matsumoto M, Maeda R. Ultrasonic micromixer for mixfofluidic systems. *Sens Actuators A, Phys*. 2001; 93:266–272.
18. Chung YC. Order-changing microfluidic mixer, U.S. Patent No. 6,331,073 B1, 2001.
19. Tabeling P, Chabert M, Dodge A, Jullien C, Okkels F. Chaotic mixing in cross-channel micromixers. *Phil Trans R Soc Lond A*. 2004; 362:987–1000.

20. Li X, van der Steen G, van Dedem GWK, van der Wielen LAM, van Leeuwen M, van Gulik WM, Heijnen JJ, Krommenhoek EE, Gardeniers JGE, van den Berg A, Ottens M. Improving mixing in micro bioreactors. *Chem Eng Sci*. 2008;63:3036–3046.
21. Krommenhoek EE, van Leeuwen M, Gardeniers JGE, van Gulik WM, van den Berg A, Li X, Ottens M, van der Wielen LAM, Heijnen JJ. Lab-scale fermentation tests of micro chip with integrated electrochemical sensors for pH, temperature, dissolved oxygen, and viable biomass concentration. *Biotechnol Bioeng*. 2008;99:884–892.
22. Suriani AR, Pitts B, Stewart PS. Rapid diffusion of fluorescent tracers into *Staphylococcus epidermidis* biofilms visualized by time lapse microscopy. *Antimicrob Agents Chemother*. 2005;49:728–732.
23. Bird RB, Stewart WE, Lightfoot EN. *Transport Phenomena*. Wiley: New York, 2001.
24. WolframMathWorld. Available at: http://mathworld.wolfram.com/HeavisideStepFunction.html, 2009.
25. Verduyn C, Postma E, Scheffers WA, van Dijken JP. Effect of benzoic acid on metabolic fluxes in yeasts—a continuous-culture study on the regulation of respiration and alcoholic fermentation. *Yeast*. 1992;8:501–517.
26. Dutta D, Ramachandran A, Leighton DT Jr. Effect of channel geometry on solute dispersion in pressure-driven microfluidic systems. *Microfluid Nanofluid*. 2006;2:275–290.
27. Taylor GI. Dispersion of soluble matter insolvent flowing slowly through a tube. *Proc R Soc Lond*. 1953;219A:186–203.
28. Beard DA. Taylor dispersion of a solute in a microfluidic channel. *J Appl Phys*. 2001;89:4667–4669.
29. Wooding RA. Instability of a viscous liquid of variable density in a vertical Hele-Shaw cell. *J Fluid Mech*. 1960;7:501–515.
30. Doshi MR, Daiya PM, Gill WN. Three dimensional laminar dispersion in open and closed rectangular conduits. *Chem Eng Sci*. 1978;33:795–804.
31. Guell DC, Cox GR, Brenner H. Taylor dispersion in conduits of large aspect ratio. *Chem Eng Commun*. 1987;58:231–244.
32. Hofland GW, Berkhoff MR, Witkamp GJ, van der Wielen LAM. Dynamics of isoelectric precipitation of casein using sulfuric acid. *AIChE J*. 2003;49:2211–2223.

Manuscript received May 26, 2008, and revision received Feb. 12, 2009.